

Near-seismic effects in ULF fields and seismo-acoustic emission: statistics and explanation

O. Molchanov¹, A. Schekotov¹, M. Solovieva¹, E. Fedorov¹, V. Gladyshev¹, E. Gordeev², V. Chebrov³, D. Saltykov³, V. I. Sinitsin³, K. Hattori⁴, and M. Hayakawa⁵

¹Inst. of the Physics of the Earth, Russian Academy of Sciences, Bolshaya Gruzinskaya 10, 123995, Moscow D-242, Russia

²Inst. of Volcanology, Petropavlovsk-Kamchatski, Kamchatka, Russia

³Inst. of Geophysical Survey, Russian Academy of Sciences, Far-East Branch, Petropavlovsk-Kamchatski, Kamchatka, Russia

⁴Marine Biosystems Research Center, Chiba University, 1-33, Yayoi, Chiba 263-8522, Japan

⁵University of Electro-Communications, Chofu 1-5-1, Tokyo 182, Japan

Received: 20 July 2004 – Revised: 10 November 2004 – Accepted: 12 November 2004 – Published: 3 January 2005

Part of Special Issue “Precursory phenomena, seismic hazard evaluation and seismo-tectonic electromagnetic effects”

Abstract. Preseismic intensification of fracturing has been investigated from occurrence analysis of seismo-acoustic pulses (SA foreshocks) and ULF magnetic pulses (ULF foreshocks) observed in Karimshino station in addition to seismic foreshocks. Such analysis is produced for about 40 rather strong and nearby isolated earthquakes during 2 years of recording. It is found that occurrence rate of SA foreshocks increases in the interval (–12, 0 h) before main shock with 3-times exceeding of background level in the interval (–6, –3 h), and occurrence probability of SA foreshocks ($p_A \sim 75\%$) is higher than probability of seismic foreshocks ($p_S \sim 30\%$) in the same time interval. ULF foreshocks are masked by regular ULF activity at local morning and daytime, nevertheless we have discovered an essential ULF intensity increase in the interval (–3, +1 h) at the frequency range 0.05–0.3 Hz. Estimated occurrence probability of ULF foreshocks is about 40%. After theoretical consideration we conclude: 1) Taking into account the number rate of SA foreshocks, their amplitude and frequency range, they emit due to opening of fractures with size of $L=70\text{--}200\text{ m}$ ($M=1\text{--}2$); 2) The electro-kinetic effect is the most promising mechanism of ULF foreshocks, but it is efficient only if two special conditions are fulfilled: a) origin of fractures near fluid-saturated places or liquid reservoirs (aquifers); b) appearance of open porosity or initiation of percolation instability; 3) Both SA and ULF magnetic field pulses are related to near-distant fractures ($r < 20\text{--}30\text{ km}$); 4) Taking into account number rate and activation period of seismic, SA and ULF foreshocks,

it is rather probable that opening of fractures and rupture of fluid reservoirs occur in the large preparation area with horizontal size about 100–200 km.

1 Introduction

Fracturing is a basic process in the Earth's lithosphere. Traditional analysis of fracturing is registration of seismic pulses (shocks) at the ground surface. Famous Gutenberg-Richter law describes averaged occurrence rate of the fracturing. It states that number of opening fractures in the time unit ($N_t = \partial N / \partial t$) depends mainly on the magnitude M or linear size of the fracture L and on level of the regional tectonic activity A ; dependence on L shows distribution with fractal exponent $c=2b+1$, $b \sim 0.9$ (see discussion later). Thus, in the seismo-active area like Japan the large fractures ($M=6\text{--}7$, $L=10\text{--}50\text{ km}$), usually treated as noticeable earthquakes, occur several times per year while moderate fractures ($M=3\text{--}4$, $L=0.5\text{--}2\text{ km}$) occur several times per day. Slow variations of N_t are usually attributed to tectonic activation or quiescence and have a scale of years. Faster intensifications of fracturing with scales of several days or even several hours are also well-known, they occur in the time vicinity of large earthquakes as aftershock or foreshock series. Mogi (1985) defined three types of such a variation: a) Complete sequence foreshocks-main shock-aftershocks with climax at an earthquake main shock, foreshock activity is ascending both in magnitude and number rate but aftershock activity is descending. Duration of aftershock series can be several weeks

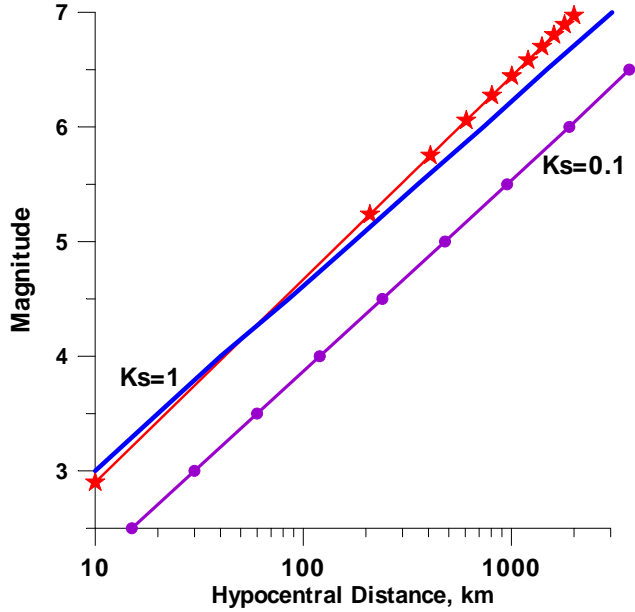


Fig. 1. Curves $K_s = K_s^* = 1$ (solid line) and $K_s = 0.1$ (line with closed circles) in coordinates M (magnitude), R (hypocentral distance). They indicate limiting distances $R^*(M)$ for earthquakes with defined value of M and threshold of sensitivity K_s^* . Each individual EQ is represented by point in this plot. The criterion $K_s > K_s^*$ means that EQ points above these curves are included into consideration. Limiting distances from observation of seismo-acoustic emission at Matsushiro station in Japan (Gorbatikov et al., 2002) are shown by curve with stars.

for large earthquakes ($M > 6-7$), but its duration is several days or less for moderate earthquakes ($M = 4-5$). Duration of foreshock series is shorter than aftershock one; b) Incomplete sequence main shock- aftershocks when foreshock series is absent and the earthquake looks as a sudden event. c) Ascending (foreshock) and descending (aftershock) series of moderate earthquakes without clear climax, so-called earthquake swarm. It looks as incomplete sequence without large main shock while its usual duration is several weeks. Unfortunately, the occurrence probability of the complete sequence is not very high (20–30%; Scholz, 1990) and a question immediately arises whether an earthquake with sudden start is a regular phenomenon or the absence of foreshocks is due to lack of the seismometer sensitivity. The next question is an origin of the sequence itself. As concerns aftershocks, they are usually explained by residual relaxation of strain-stress increase generating a main shock. Inverse process of the stress accumulation and related dilatancy could be in principle responsible for appearance of foreshocks as it was discussed in numerous papers some times ago (see e.g. discussion in Scholz, 1990). However, it has been recently discovered that the value of stress increase or stress drop caused by an earthquake is not so large and dilatancy fracturing due to stress accumulation is negligible. It leads sometimes to conclusion that there is no preparatory (precursory) stage of an earthquake (Main, 1997). Obviously, this

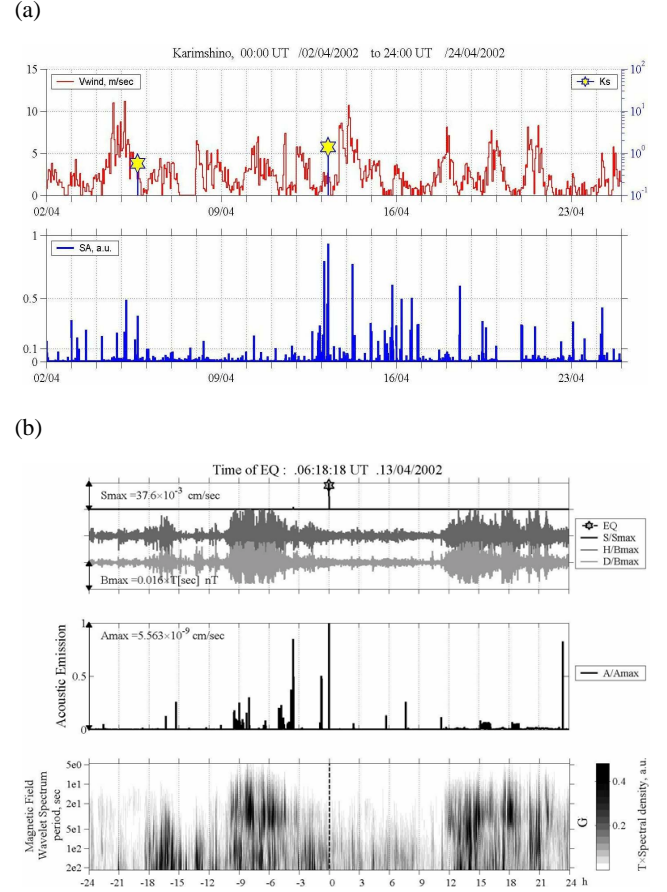


Fig. 2. (a) SA pulses ± 12 days from 13 April 2002 EQ ($M = 4.9$, $D = 128$ km, $H = 45$ km, $K_s = 1.4$). Upper panel: yellow stars are time and K_s value of 13 April 2002 EQ, and the weaker EQ which happened 8 days before ($K_s = 0.5$) together with variation of atmosphere wind velocity. Lower panel: Amplitudes of SA pulses (in arbitrary units). There is some known correlation with atmosphere wind but a connection with EQ-s is also seen. (b) SA and ULF observational results in the vicinity (± 24 h) of the earthquake 13 April 2002 ($M = 4.9$, $D = 128$ km, $H = 45$ km, $K_s = 1.4$) happened in day-time (16:48 LT). Upper panel presents recording of seismometer: amplitude of the EQ shock (star) and weak foreshock about 4 h ahead. Next panel shows the intensity of ULF magnetic field variations in the frequency band 0.003–0.1 Hz (NS and EW horizontal components). Third panel from above shows the intensity of pulsating SA signal and last panel shows the wavelet spectrum of ULF horizontal component intensity.

conclusion is not stimulating to solve the main problem of seismology, the forecast of damaging earthquakes. In such a situation observation of nonseismic phenomena could be helpful to validate the precursory fracturing. We discuss here two types of such events: seismo-acoustic (SA) pulsating emission and ULF magnetic field variations registered at the Russian-Japanese complex observatory Karimshino (Uyeda et al., 2002). Indeed, the SA observation is an extension of traditional seismic recording to the high-frequency range ($F > 10$ Hz). As a result, we can improve the sensitivity for

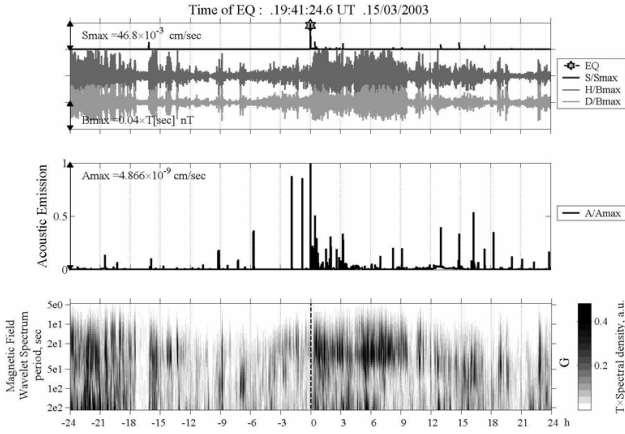


Fig. 3. The same as in Fig. 2b but for EQ 15 March 2003 ($M=6.4$, $D=187$ km, $H=5$ km, $K_S=26.1$, which happened at morning time (06:12 LT).

small-size fracturing but lose a possibility to detect signals from far-distant areas (see Sect. 5). There are a lot of reports on wide-band SA emission before large earthquakes. For example Morgunov et al. (1991) recorded a distinctive anomaly in SA noise behavior in the range $F=800\text{--}1200$ Hz about 16 h before the famous $M=7.0$ Spitak earthquake, Armenia, 1988, at the distance 80 km from the epicenter. Gorbatikov et al. (2002) found an increase of the SA intensity averaged over 20 min in the frequency range from $F=25$ Hz to $F=1000$ Hz in a time 2–12 h before several moderate earthquakes ($M=4\text{--}5$) at the Matsushiro station in Japan. They discovered that the frequency channel $F=25\text{--}35$ Hz is the most sensitive to seismicity. Unlike them, we are going to analyze pulsating component of SA signals (Sects. 3 and 4). Three types of ULF electromagnetic signals associated with earthquakes have been reported till now. The first (in time interval \pm several minutes around main shock) is a co-seismic signal (e.g. Eleman, 1965; Takeuchi et al., 1997), which appears just after the shock and probably is initiated by strong seismic pulse induction (Surkov et al., 1999; Molchanov et al., 2001), it is hardly connected with preseismic fracturing. The second type is preseismic noise-like ULF magnetic field emission in the time interval several days or weeks before large earthquakes (Fraser-Smith et al., 1990; Haykawa et al., 1996; Kopytenko et al., 2002). However, a relation of this emission to preseismic fracturing is not proved. Moreover, our observations in Karimshino showed a clear depression of ULF magnetic field intensity several days before the earthquakes. The effect is probably connected with seismo-induced perturbations in the atmosphere-ionosphere and evidently has no relation to the foreshock activity (Molchanov et al., 2003). Therefore, we pay attention to the third type of ULF signals, so-called near-seismic ULF magnetic field pulses in the time interval several hours ahead of the main shock. A well-known case of such an event is so-called ULF magnetic emission 2–3 h before large Spitak earthquake (Molchanov et al., 1992; Kopytenko et al., 1993)

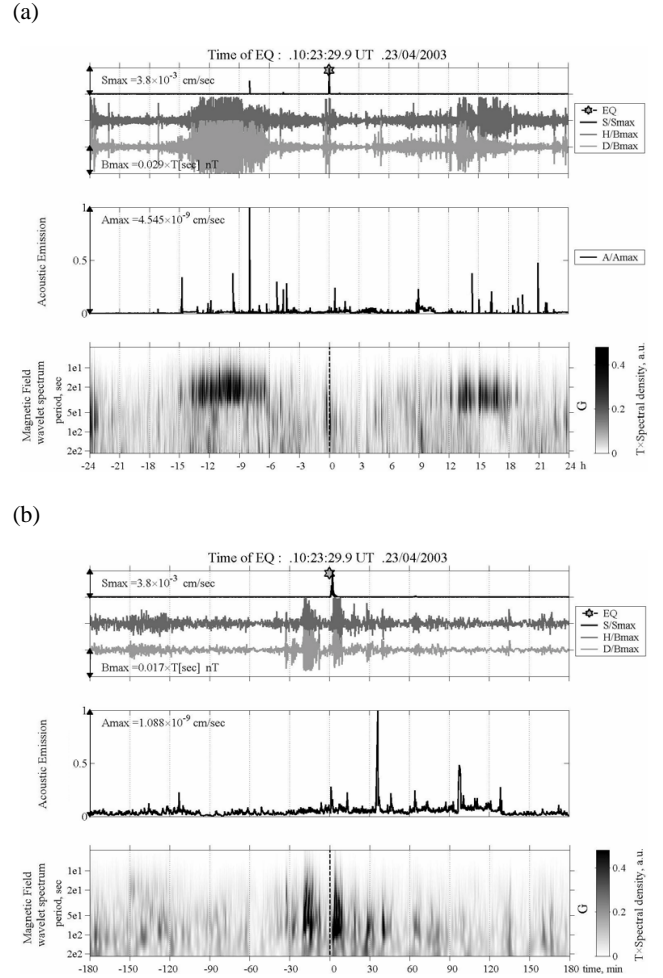


Fig. 4. (a) The same as in Fig. 2b but for EQ 23 April 2003 ($M=5.8$, $D=485$ km, $H=10$ km, $K_S=1.5$), which happened at late evening time (20:53 LT). (b) Extension of the (a) to the interval ± 3 h from the seismic shock.

2 Equipment and seismic index

During 1999–2000, in addition to the existing seismic and geophysical observations, Russian and Japanese scientists established a special observatory at Karimshino site (52.94° N, 158.25° E) in Kamchatka (Far-Eastern Russia). Its main purpose is to study a correlation of seismic activity with electromagnetic and other nonseismic phenomena. The main advantage of this station is quiet electromagnetic environment that allows us to use rather sensitive equipment and to check some theoretical ideas. The regular recordings have been started since June 2000 and some information about Karimshino station is already published (Uyeda et al., 2002; Molchanov et al., 2003).

Our three-component induction magnetometer measures the geomagnetic field variations in the frequency range 0.003–40 Hz. The sensitivity threshold is better than $20 \text{ pT/Hz}^{1/2}$ at frequency 0.01 Hz. It corresponds to $0.02 \text{ pT/Hz}^{1/2}$ at frequencies above 10 Hz. Since September

Table 1. Main parameters of the registration.

1 Date	2 <i>M</i>	3 Distance km	4 <i>K_s</i>	5 <i>H</i>	6 <i>Az</i>	7 UT	8 Seism forsh	9 <i>T</i> seism	10 SA forsh	11 <i>T</i> SA forsh	12 ULF	13 <i>T</i> ULF	14 ULF spectr.
8 Oct. 2001	6.5	155	39.1	26	97	18.14	2	20	> 5	20	+	6	
13 Nov. 2001	6.6	749	6.1	13	86	10.43	2	20	> 10	21	+	2	HF ULF
25 Nov. 2001	4.5	115	4.5	22	137	10.36	0		2	6	+	1	
15 Dec. 2001	4.8	64	1.5	91	170	1.59	0		> 10	12	day		
28 Jan. 2002	5.8	421	1.9	77	-164	13.5	0		> 5	10	+	2	
15 Feb. 2002	5.1	141	2.1	20	124	15.21	2	21	> 10	21	-		
13 Apr. 2002	4.9	128	1.4	45	82	6.18	0		> 10	15	day		HF ULF
26 Apr. 2002	5.8	192	6.8	43	69	7.15	1	7	3	6	day		
3 May 2002	5.2	194	1.6	10	105	3.04	2	3	>10	5(23)	day		HFULF
8 May 2002	5.8	167	8.5	21	113	4.12	0		3+noise	6	day		
31 May 2002	6.1	842	1.1	10	91	6.09	0		> 10	10	day		
8 Sept. 2002	5.5	379	1	53	-169	5.2	0		> 10	23	day		HFULF
8 Oct. 2002	5	151	1.5	27	97	9.18	0		>5+noise	18	-		
16 Oct. 2002	6	132	12.5	113	-175	10.12	0		0		+	1	
20 Oct. 2002	5	150	1.5	29	89	1.34	0		2	4	day		
18 Dec. 2002	5	113	2.2	42	82	11.09	0		> 5	15	-		
1 Jan. 2003	4.9	145	1.2	29	92	1.33	1	20	> 5	20	day		HF ULF
6 Feb. 2003	5.1	147	1	159	163	4.42	0		> 10	22	day		
15 Mar. 2003	6.4	187	26.1	5	116	19.41	1	16	> 10	21	+	1	
19 Mar. 2003	6.2	191	16.8	5	110	14.42	4	13	> 10	16	-		
25 Mar. 2003	5.1	189	1.3	17	116	13.24	1	1	> 10	13	-		
23 Apr. 2003	5.8	485	1.5	10	46	10.23	1	8	> 10	15	+	0.5	
17 May 2003	5	181	1.1	16	135	1.46	1	6	>5	21	day		
12 Aug. 2003	5.1	191	1.3	5	161	11.45	0		3	19	-		

Legend:

1. Date of selected strong and nearby earthquake ($K_s \geq 1$)
2. Magnitude of the earthquake.
3. Epicenter distance, km.
4. K_s index.
5. Hypocenter depth, km.
6. Azimuth calculated from the North direction clockwise
7. Universal time (LT= UT + 10^h30^m)
8. Number of seismic foreshocks during a day before the earthquake.
9. Time of the first seismic foreshock, hours before earthquake.
10. Number of SA foreshocks.
11. Time of the first SA foreshock, hours.
12. Presence of ULF foreshocks (+) or strong morning-day time ionosphere-magnetosphere emission (day) several hours before earthquake.
13. Time of the first ULF foreshock, hours.
14. Specific high-frequency ($F=1-4$ Hz) ULF spectrum changes before earthquake.

2001 in addition to wide-band SA receiver (accelerometer type) we have installed a resonant SA receiver, which is tuned near frequency $F=30$ Hz. It has high sensitivity for pulsating seismo-acoustic signals (Saltykov et al., 1998).

Here we analyze ULF magnetic and SA data during 2 years of regular observations from 1 September 2000 to 1 October 2003. A parameter characterizing seismic influence is necessary for the correlation analysis of seismic and non-seismic data. The seismic characteristics, such as magnitude M , epicenter distance D , depth H , are presented in seismic catalogues. We assume that the index of seismic activity is proportional to seismic energy input $\Delta E_s = \int P_s dt \sim \langle P_s \rangle \tau$, where P_s is seismic energy flux and τ is duration of seismic pulse. P_s is decreasing with distance due to divergence

of flux in space ($\sim R^{-2}$), inelastic attenuation (coefficient F_a) and scattering or elastic attenuation (Aki and Richards, 1980). Scattering can be described in terms of multi-ray propagation and in the first approximation the scattering factor in P_s is inversely proportional to τ . Hence:

$$\Delta E_s \cong \left(E_s / R^2 \right) F_a \sim (10^{1.5M} / R^2) F_a(R, M), \quad (1)$$

where Kanamori and Anderson (1975) scaling is used and $R = (D^2 + H^2)^{1/2}$.

We introduce a seismic index K_s as following (Molchanov et al., 2003):

$$K_s = \sqrt{\Delta E_s / \Delta E_s^*} = 10^{0.75M} \Phi_a / (10R), \quad (2)$$

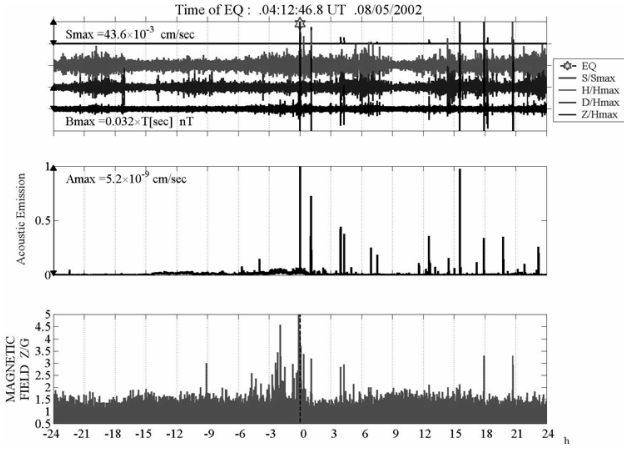


Fig. 5. Results of data analysis in the case of the EQ on 8 May 2002 ($M=5.8$, $D=167$ km, $H=21$ km, $K_s=8.5$, $LT=14:42$). Upper panel is seismic recording, next panel is ULF intensity in the frequency range $F=1-4$ Hz for all 3 components of the magnetic field variation, then it is SA signal amplitude, and at the last panel impedance ratio Z/G is shown for the same HF ULF frequency range as in the second panel.

where $\Phi_a = \sqrt{F_a} \cong (1 + 2R/L_a)^{-2.66}$. Here L_a is attenuation distance and it is easy to find that $L_a \cong QL \cong 2 \times 10^{M/2}$ (km), where $Q \cong 100$ is elastic quality and L is average size of the seismic source (Aki and Richards, 1980).

The dependencies for $K_s=1$ and $K_s=0.1$ in M , R coordinates are presented in Fig. 1. In such a presentation the line R (M , $K_s = \text{constant}$) shows the limiting distance for a given threshold $K_s^* = \text{constant}$ determined by mechanisms of nonseismic effects and sensitivity of a receiver. Recently Gorbatiokov et al. (2002) reported about the bursts of seismo-acoustic emission (SAE) registered at Matsushiro station (Japan) in association with rather large seismic shocks ($M=3-5$). They found that a separatrix occurs between earthquakes accompanied by SAE bursts and earthquakes without SAE bursts if the results are plotted in M - R diagram. The equation of the separatrix is written as follows

$$M = M(R^*) = 1.77 \log R^* + 1.13. \quad (3)$$

This dependence is also depicted in Fig. 1. It is evident that the limiting distance enlarges when K_s decreases. Change of K_s -threshold from 1 to 0.1 leads approximately to 3-times distance enlargement and about $(K_s^*)^{-1}$ increase of reception area.

3 Case study

In order to exclude aftershock series and swarms we have selected only strong and nearby earthquakes ($K_s \geq 1$), with no strong preceding shocks ($K_s > 0.5$) for at least 3 days. We have found 25 such earthquakes with magnitude from $M=4.5-6.5$. Main parameters of the earthquakes are presented in Table 1. Example of SA data in the time span of ± 12 days around 13 April 2002 EQ ($M=4.9$, $D=128$ km,

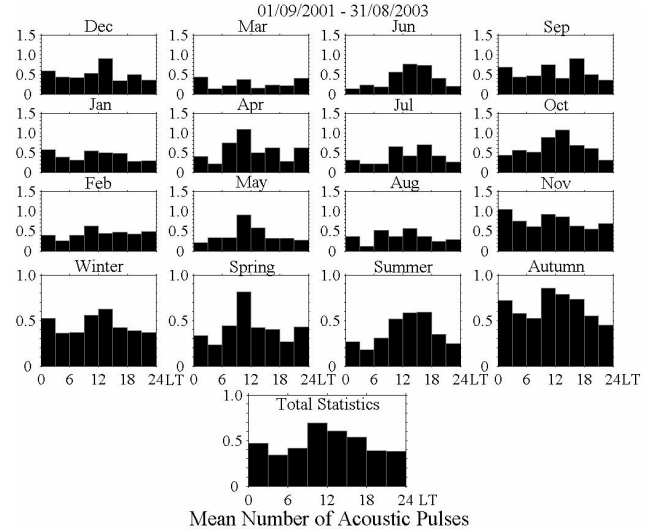


Fig. 6. Averaged number of SA pulses/(per 3 h) = N_A in dependence on local time and for different seasons.

$H=45$ km, $K_s=1.4$, row 7 in Table 1) is shown in Fig. 2a together with variation of atmosphere wind velocity, which is one of the main SA induction sources. SA and ULF observational results in the interval ± 24 h from time of the shock are shown in Fig. 2. Both foreshock and aftershock series are absent in seismometer recording in this case (except one weak foreshock 4 h ahead) but SA foreshock series do exist. As for ULF magnetic field signals, we can not find clear connection with seismic shocks due to daily variation of ULF intensity related mainly to magnetic pulsations from ionosphere and magnetosphere. These magnetospheric signals appear usually at morning-day time (e.g. Ansari and Fraser, 1986; see also next section) and can mask the signals from underground. An other example is shown in Fig. 3. The same as before, foreshock series in seismometer recording are absent but the SA foreshocks are clearly seen. ULF response is also questionable here probably due to morning time of observation. However, in the case presented in Fig. 4, in which seismic shock happened at evening time, some unusual pulses about 1 h before seismic shock can be supposed.

Note that unlike spectrum of morning-day time magnetic pulsations from ionosphere-magnetosphere with periods 20–30 s (see Fig. 4a), the ULF signals suspected for association with earthquake have more wide-band spectrum, which stretches from periods 100–150 s to about 1 s (Fig. 4b). It is interesting also that total duration of the ULF pulse is about 10 min and internal structure with shorter pulses of about 1 min duration can be seen.

In attempt to find some signature of ULF foreshocks even in morning-day time we have tried to analyze high-frequency part of ULF spectrum ($F=1-4$ Hz) and calculate impedance ratio Z/G (Z is vertical component intensity of the ULF field, $G=EW+NS$ is total horizontal intensity). Efficiency of the impedance analysis is known in application to pre-seismic ULF noise-like emission (Hayakawa et al., 1996;

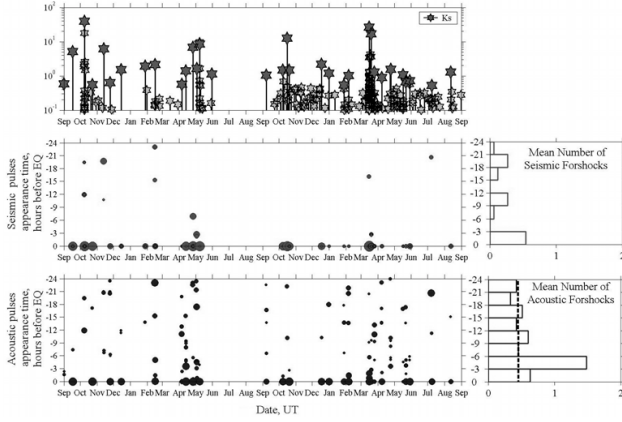


Fig. 7. (a) Upper panel: Seismic activity in terms of K_S values during 2 years of observation. Distribution of averaged number of pulses during 1 day before strong seismic shocks ($K_S \geq 0.5$) for seismic foreshocks (middle panel) and for SA foreshocks (panel below). Amplitude of the foreshock is proportional to size of the black circle. Aftershock influence is excluded by selection (see text). Distribution averaged on 33 strong and nearby earthquakes is shown on right. Background level of N_A pulses is shown by dash line.

Molchanov et al., 2003). An example of the analysis is presented in Fig. 5. While the result seems interesting, we have found that this type of analysis is not very reliable for revelation of pulsating ULF activity due to presence of atmospheric pulses from thunderstorms and man-made interferences in Z-component. Nevertheless we include these results in Table 1.

4 Statistics

Let us estimate the statistical properties of nonseismic foreshocks. Taking into account that SA pulses can be generated not only by fracturing but also by atmosphere winds, tides, temperature and man-made sources (Gordeev et al., 1991; Saltykov et al., 1998) we find firstly overall average occurrence rate of SA pulses. Diurnal and seasonal variations of the number of impulses with amplitudes higher than double averaged amplitude N_A are shown in Fig. 6. It can be seen that averaged $N_A \approx 0.5$. Then we plot averaged N_A in the interval $(-24 \text{ h}, 0)$ before selected seismic strong and nearby earthquakes ($K_S \geq 0.5$, 33 seismic events) in Fig. 7a. As before (see description of Table 1 in the previous section), we exclude the aftershock influence. It is evident that in the interval $(-6 \text{ h}, -3 \text{ h})$ N_A exceeds background level about 3 times and total interval of SA foreshock intensification is about 12 h before a seismic shock. In order to be sure that the result is reliable, we estimate the confidence intervals of the distribution and in addition the distribution of SA pulses for random selection of 33 event dates both in the interval of 2 years and in the interval of three months from 1 June 2002 to 31 August 2002, when earthquake activity is weak (see Fig. 7a). These estimates are presented in Fig. 7b. We think they demonstrate non-coincidental relation of SA foreshock intensification to selected strong and nearby seismic shocks.

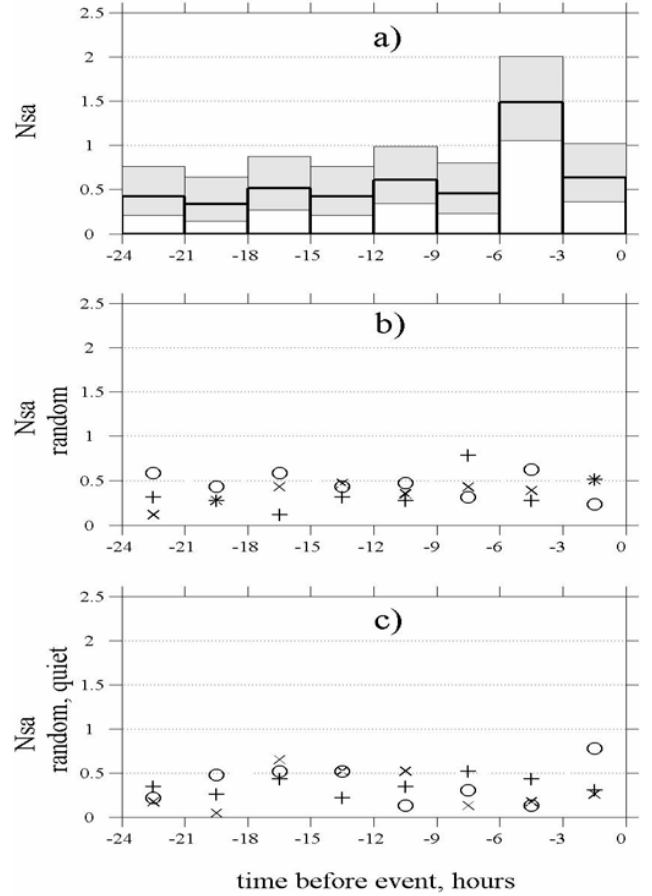


Fig. 7. (b) Panel a): Averaged distribution of SA pulses 1 day before 33 strong and nearby seismic events (the same as on right of (a) but with indication of 98% confidence intervals by grey rectangular up and down. Thick lines are mean values). Panel b): Mean number of SA pulses in eight 3 h intervals before events for 3 independent samples with random event time (33 events in each sample from 1 September 2001 to 31 August 2003). Panel c): Mean number of SA pulses in eight 3 h intervals before events for 3 independent samples with random event time for quiet interval (33 events in each sample, from 1 June 2002 to 31 August 2002).

In fact, our estimation is similar to known BSR (boot strap resembling) method, when the statistics is not robust as in our case.

Background daily ULF magnetic field variation and averaged spectrum are presented in Fig. 8. As expected, this variation is maximal in the morning-day interval 06:00–16:00 LT and it is related mainly to Pc-3 magnetospheric pulsations in the characteristic frequency range 0.02–0.04 Hz. Then, taking into consideration that the ULF pulses are usually longer than short SA pulses, their amplitude is comparable with background noise and total interval of suspected ULF pulses is shorter than 6 h (see Table 1), we produce analysis of averaged ULF intensity in $(-12 \text{ h}, 0)$ period before selected seismic shocks. The result is shown in Fig. 9. We calculate normalized horizontal intensity $\langle (G - G_{av}) / G_{av} \rangle$ for each 0.5 h subinterval, where G_{av} is the ULF intensity averaged

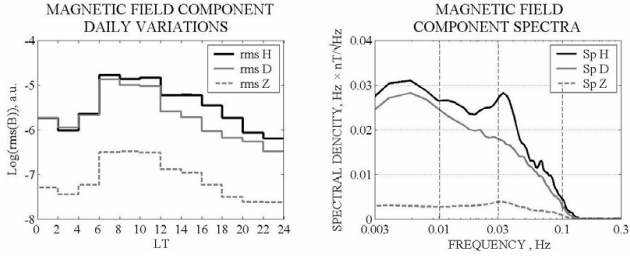


Fig. 8. Averaged overall ULF magnetic field daily variation and spectrum.

over 3 days before the seismic shock. We conclude that a reliable intensification of ULF intensity (about 3 times above background variation) occurs in the time interval $(-3\text{ h}, +1\text{ h})$ when $K_s \geq 1$.

Now we estimate the occurrence probability of SA and ULF foreshocks. Number of background SA pulses in the interval 12–15 h before EQ is about 2–2.5 (see Figs. 6 and 7). Referring to Table 1, we can consider each case with number of SA foreshocks more than 5 as the case of fracturing intensification. Because we have 19 such cases from 25, our estimation of SA foreshock occurrence probability is $p_A=76\%$. If we define the seismic foreshock series as occurrence of more than one pulse during one day before earthquake, then it can be seen from Table 1 that occurrence probability of seismic foreshocks is 20%, but if we take into account each foreshock event, then seismic foreshock probability is $p_s=44\%$ (11 events from 25). Similar estimation of ULF foreshock probability is hampered by above-mentioned magnetic pulsation intensification in morning-day time. ULF probability during nighttime is $p_m=28\%$. However, if we take into account ULF foreshock findings in Table 1 both in amplitude variation in the frequency range $F \leq 0.1\text{ Hz}$ and in HF ULF range ($F=1\text{--}4\text{ Hz}$), then ULF probability is $p_m=44\%$.

5 Discussion

Our results demonstrate that absence of seismic foreshocks for earthquake with sudden inclusion does not mean absence of earthquake preparation stage. Thus, the existence of definite precursory process is in compliance with not only common sense but also with observational evidences.

We use the index K_s and corresponding limiting distance of the preparation zone $R(M, K_s)=R^*$ (see Fig. 1) as characteristics of precursory process. It looks as deterministic assumption. However, it can be considered as a result of averaging on ensemble of more or less individual earthquake events. Note that for $K_s \sim 1$, $R^* \sim L_a/2$ (L_a is the seismic attenuation distance, $L_a=QL \cong 2 \times 10^{M/2}$, then observational relationship (Eq. 3) can be reduced to $R^* \cong 0.23 \cdot 10^{0.56M} \cong 0.23 \cdot 10^{0.06M} L_a/2$. It means that the size of preparation zone is approximately equal to the distance of resultant distribution of seismic energy. The spec-

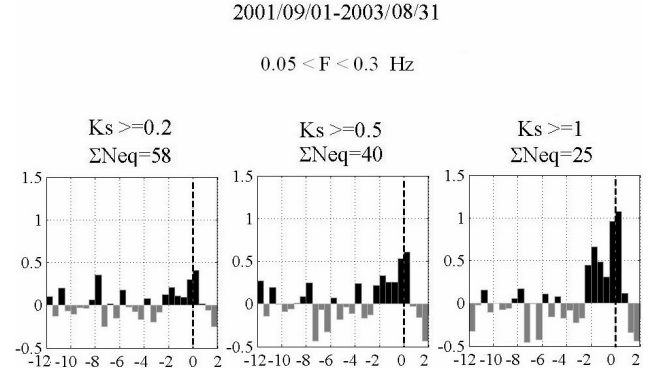


Fig. 9. Distribution of normalized ULF horizontal component intensity in the frequency range $F=0.05\text{--}0.3\text{ Hz}$ for different ensembles of selected earthquake shocks with different thresholds and in the interval 12 h before and 2 h after each shock.

trum of seismic or SA pulse is the following (see e.g. Molchanov et al., 2002):

$$(\partial u/\partial t)_\omega = u_0 C_s \sqrt{\tau/2\pi} / (\pi r) x^2 (1+x^2)^{-3/2} \exp(-xr/La), \quad (4)$$

where is final slip ($\approx 10^{-4}L$), $x=\omega\tau_0$, $\tau_0=L/(2C_r)$, $C_s \approx C_r$ are velocities of seismic wave and rupture. The spectrum depends on distance r and size L , Fig. 10, and for distances $r \ll L_a$ the spectrum maximum is near $x=\sqrt{2}$ or $F=F_m=\sqrt{2}C_r/(\pi L) \approx 1350/L$ (m) Hz.

It is obvious that, unlike conventional seismometer, the SA narrow-band receiver is sensitive to opening of small fractures with size from 20 to 200 m (values M from 0 to 2), the reception distances (or attenuation distances) for such fractures lie between 5 and 20 km.

As for ULF foreshocks, we take into account three known models of electromagnetic field generation due to fracturing: the first is CR model, in which charge relaxation during fracture opening is considered (Gershenzon et al., 1989; Molchanov and Hayakawa, 1995); the second (EKE) model is based on mechanism of electro-kinetic conversion in a course of water diffusion just after crack opening in order to compensate changes in high pore pressure around crack (Mizutani et al., 1976; Jouniaux and Pozzi, 1995; Fenoglio et al., 1995) and the third is model of inductive electromagnetic pulses (IP) arising in a course of seismic wave propagation inside the conductive ground medium. This model was proposed by Surkov (1999) and also discussed by Molchanov et al. (2001) for explanation of co-seismic ULF magnetic and electric field variations. Estimations of the mechanisms efficiency for rather realistic values of parameters in terms of the current moments are in Fig. 11.

It can be seen that EKE mechanism is the most promising one at least for moderate sizes $L=50\text{--}200\text{ m}$, revealed from SA foreshocks. However, it is only efficient if two special conditions are fulfilled: a) origin of fractures near fluid-saturated places or liquid reservoirs (aquifers); b) appearance of open porosity or initiation of percolation instability (Fenoglio et al., 1995; Jouniaux and Pozzi, 1995).

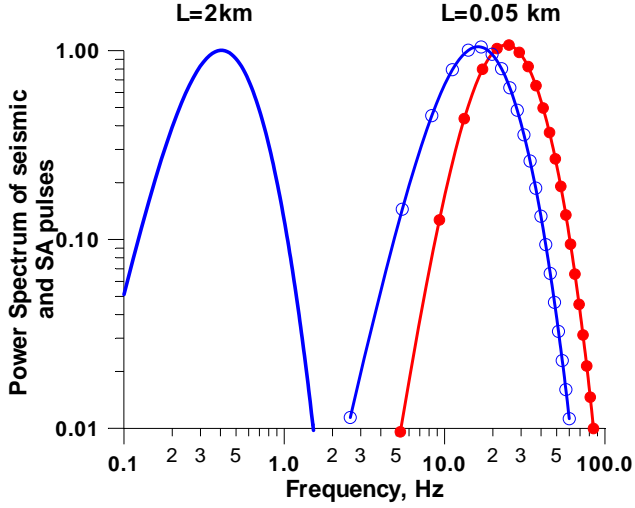


Fig. 10. Power spectrum of seismic shock in dependence on fracture size $L=2$ km ($M \approx 4$), solid line and $L=50$ m ($M \approx 1$), line with open circles (recording of deformation velocity) or line with closed circles (accelerometer). Both spectrums are at the distance of seismic attenuation ($r=L_a \approx 100L$).

Let us consider now a possibility of noise-like SA or ULF fracturing emission. It depends on occurrence rate of fracturing. Background number rate of seismic pulses in the range of magnitudes from $M \sim 7$ to about $M \sim 3$ is described by Gutenberg-Richter relationship:

$$N_t(L_* \leq L) = A(L_*)^{-2b}. \quad (5)$$

It means that number rate density is as follows:

$$\partial N_t / \partial L(L, L+dL) = 2bA(L)^{-(2b+1)}. \quad (6)$$

Usually accepted value of constant $b \approx 0.9$. This value is keeping approximately during fracturing intensification. It was found (Evernden, 1986) from observation of many after-shock series that $b=0.7-1.2$, therefore we suppose the same distribution in foreshock series but extend it for smaller L values by simple assumption concerning size-volume density:

$$\partial^2 N_t / \partial V \partial L = B(r) / L^c. \quad (7)$$

Number density in the point of observation r_0 is the following:

$$\partial N_t / \partial L = \int_{V_f} \partial^2 N_t / \partial V' \partial L \exp(-R/La) dV'. \quad (8)$$

where V_f is a region of fracturing intensification, $R=|r_0-r'|$ and we assume for simplicity an exponential model of limiting factor with $R^* \sim La = QL$. In a case of far-distant activation region: $R \gg (V_f)^{1/3}$, $\partial N_t / \partial L = \langle B \rangle V_f \exp(-\langle R \rangle / QL) / L^c$. By comparing with Eq. (6) we find immediately that for $L > R/Q$, $\langle B \rangle V_f = 2bA$ and $c = 2b + 1 \approx 2.8$. Note that assumption (Eq. 7) with $c \approx 3$ corresponds to so-called L^{-3} criterion,

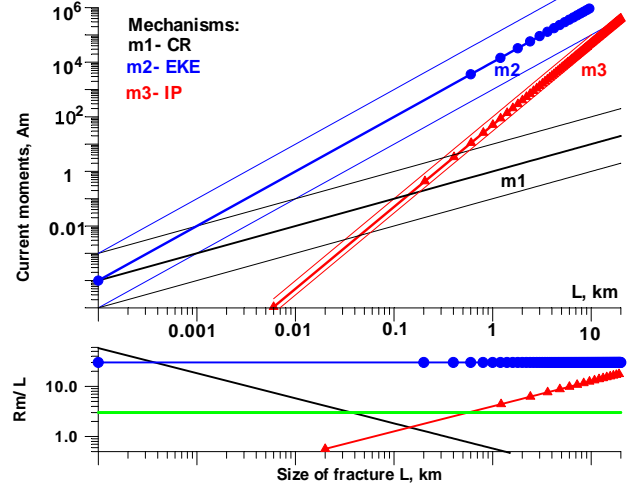


Fig. 11. Above panel: estimation of current moments of different ULF generation mechanisms in dependence of fracture size L , CR model is solid line, EKE model is line with closed circles, IP model is line with triangles (see text for description of the models). Below: normalized reception distance for different models.

which was exploited in many papers on fracturing emission (e.g. Gershenzon et al., 1989). However, in a case of far-distance activation area we cannot expect any pulses from small-size fractures as it is shown in Fig. 12. Let us suppose now that the activation region is so large that includes near-distant sites and B does not depend on distance critically. In a case of flattened out cylinder with characteristic horizontal size $D_0 \sim 100$ km and vertical size $H \sim 10$ km, which is about depth of the crust, the approximated Eq. (8) can be re-written as follows

$$\partial N_t / \partial L \approx \langle B \rangle V_0 L^{3-c} / \left[(L^2 + D_0^2 / Q^2)(L + H/Q) \right], \quad (9)$$

where $V_0 = \pi D_0^2 H$. The result both for number rate density and cumulative number rate together with observational values N_t is also shown in Fig. 12.

For origin of noise-like signal we suppose a pulse overlapping or condition:

$$N_t \tau \geq 1. \quad (10)$$

It is true both for correlated and not correlated pulses. In our problem the duration of seismic pulse $\tau \approx a\tau_0 \approx aL / (2C_r)$, where a is elongation of the pulse due to elastic scattering ($a < Q$). Had dependence (Eq. 5) be valid even for smallest values of L we could expect generation of emission from opening of small fracture (crack) ensemble with size $L \leq L_e \approx aN_1 L_1^{2b} / Cr$, where $N_1 = N_t(L > L_1)$. Looking on Fig. 12 we find $N_1 \sim 10^{-5}$ s for $L_1 \sim 2$ km, in result $L_e \approx 0.01-1$ m. Just similar range of crack sizes (and corresponding range of frequency $F=1-100$ kHz) was considered in several papers on fracturing SA emission (e.g. Gershenzon et al., 1989). However, the condition (Eq. 10) can be never fulfilled for N_t dependence shown in Fig. 12.

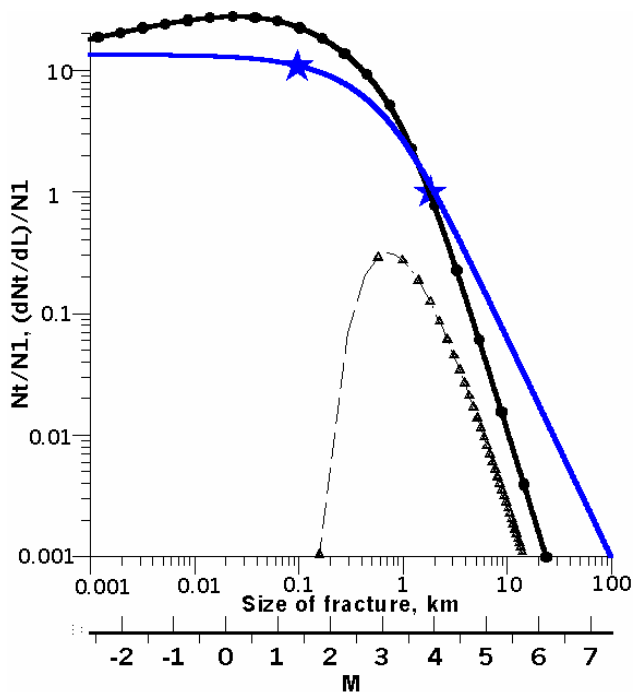


Fig. 12. Number rate density in the point of observation in a case of the far-distant region of fracturing (dash line with triangles) and in a case of large fracturing region including observation site (horizontal dimension $D_0=100$ km, thickness $H=10$ km; line with closed circles). Cumulative number rate for latter case is solid line. All the values are normalized to $N_1=N_t(L \geq 2 \text{ km}) \approx 10^{-5} \text{ s} \approx 1/\text{per day}$. Observational values are shown by stars. It is evident that model of the large activation zone is more compatible with our observation results.

The situation is different for ULF pulses generated by the EKE mechanism. In this case, the duration of pulse $\tau_m \approx L^2/(4D_w)$, where $D_w \approx (1-100) \text{ m}^2/\text{s}$ is the coefficient of water diffusion through porous ground medium (Mizutani et al., 1976; Fenoglio et al., 1995). Using the condition (Eq. 10) for values N_t in Fig. 12 it can be seen that if $L \geq 50-100 \text{ m}$ then ULF generation could be either noise-like ($D_w \sim 1 \text{ m}^2/\text{s}$) or pulsating ($D_w \sim 100 \text{ m}^2/\text{s}$). Note that large values of D_w can be explained by percolation instability (Fenoglio et al., 1995; Jouniaux and Pozzi, 1995) and limiting distances of ULF foreshocks for the same scales as related to SA pulses ($L=50-200 \text{ m}$) are 2.5–10 km (see Fig. 11).

We believe that our conclusions about the large area of fracturing activation before an earthquake and about the connection of the preparation process with unstable fluid diffusion are helpful for understanding the earthquake origin. Furthermore, the combined analysis of the fracturing intensification can be useful for earthquake forecast. For example, if we assume mild criterion of the forecast: one foreshock signature from three possible ones (seismic, SA, ULF), then supposing above-mentioned values $p_s \approx 30\%$, $p_a \approx 75\%$, $p_m \approx 40\%$, the forecast probability of EQ time is about 90%. But if we use more strict criterion: at least two type fore-

shocks from 3 possible ones, the forecast time probability is about 50%. Of course, the probability of false alarms should be taken into consideration. Therefore, a reliability of the EQ time and position forecast can be essentially improved if we develop the network of stations like Karimshino observatory.

Acknowledgements. Authors are thankful to S. Uyeda and P. F. Biagi for helpful discussion of the results. This research is performed under ISTC grant 1121.

Edited by: P. F. Biagi

Reviewed by: two referees

References

- Aki, K. and Richards, P.G.: Quantitative seismology, W. H. Freeman and Comp., San Francisco, 1980.
- Ansari, I. A. and Fraser, B. J.: A multistation study of low latitude Pc3 geomagnetic pulsations, *Planet. Space Sci.*, 34, 519–531, 1986.
- Eleman, F.: The response of magnetic instruments to earthquake waves, *J. Geomagn. Geoelectr.*, 18, 1, 43–72, 1965.
- Evernden, J. F., Archambeau, C. B., and Cranswick, E.: An evaluation of seismic decoupling and underground nuclear test monitoring using high-frequency seismic data, *Rev. Geophys.*, 2, 143–215, 1986.
- Fraser-Smith, A. C., Bernardy, A., McGill, P. R., Ladd, M. E., Helliwell, R. A., and Villard Jr., O. G.: Low frequency magnetic field measurements near the epicenter of the Loma-Prieta earthquake, *Geophys. Res. Lett.*, 17, 1465–1468, 1990.
- Gershenson, N. I., Gokhberg, M. B., Karakin, A. V., Petviashvili, N. V., and Rykunov, A. L.: Modelling the connection between earthquake preparation process and crustal electromagnetic emission, *Phys. Earth Planet Inter.*, 57, 129–138, 1989.
- Gladyshev, V., Baransky, L., Schekotov, A., et al.: Some preliminary results of seismo-electromagnetic research at Complex Geophysical Observatory, Kamchatka, in: *Seismo-Electromagnetics (Lithosphere-Atmosphere-Ionosphere Coupling)*, edited by: Hayakawa, M. and Molchanov, O., Terrapub, 2002.
- Gorbatikov, A. V., Molchanov, O. A., Hayakawa, M., Uyeda, S., Hattori, K., Nagao, T., Nikolaev, A. V., and Maltsev, P.: Acoustic emission, microseismicity and ULF magnetic field perturbation related to seismic shocks at Matsushiro station, in: *Seismo-Electromagnetics (Lithosphere-Atmosphere-Ionosphere Coupling)*, edited by: Hayakawa, M. and Molchanov, O., Terrapub, 1–10, 2002.
- Gordev, E. I., Saltykov, V. A., Sinitsyn, V. I., and Chebrov, V. N.: Effect of Earth's surface heating on high-frequency seismic noise, *Dokl. Akad. Nauk SSSR*, 316, 85–88, 1991.
- Fenoglio, M. A., Johnston, M. J. S., and Byerlee, J. d.: Magnetic and electric fields associated with changes in high pore pressure in fault zone-application to the Loma Prieta ULF emissions, *J. Geophys. Res. Solid Earth*, 100, 12 951–12 958, 1995.
- Jouniaux, L. and Pozzi, J. P.: Streaming potential and permeability of saturated sandstones under triaxial stress: Consequences for electrotelluric anomalies prior to EQs, *J. Geophys. Res.*, 100, 10 197–10 209, 1995.
- Kanamori, H. and Anderson, D.: Theoretical basis of some empirical relations in seismology, *Bull. Seismol. Soc. Am.*, 65, 1073–1095, 1975.

- Kopytenko, Yu. A., Matiashvili, T. G., Voronov, P. M., Kopytenko, E. A., and Molchanov, O. A.: Detection of ULF emission connected with the Spitak earthquake and its aftershock activity based on geomagnetic pulsations data at Dusheti and Vardziya observatories, *Phys. Earth Planet. Inter.*, 77, 85–95, 1993.
- Kopytenko, Yu. A., Ismagulov, V. S., Hattori, K., Voronov, P. M., Hayakawa, M., Molchanov, O. A., Kopytenko, E. A., and Zaitsev, D. B.: Monitoring of the ULF Electromagnetic Disturbances at the Station Network before EQ in Seismic zones of Izu and Chibo Peninsulas (Japan), in: *Seismo-Electromagnetics (Lithosphere-Atmosphere-Ionosphere Coupling)*, edited by: Hayakawa, M. and Molchanov, O., TerraPub, 11–18, 2002.
- Main, I.: Long odds on prediction, *Nature*, 385, 19–20, 1997.
- Mizutani, H., Ishido, T., Yokokura, T., and Ohnishi, S.: Electrokinetic phenomena associated with earthquakes, *Geophys. Res. Lett.*, 3, 365–368, 1976.
- Mogi, K.: *Earthquake Prediction*, Academic Press, 355, 1985.
- Molchanov, O. A., Kopytenko, Yu. A., Voronov, P. M., Kopytenko, E. A., Matiashvili, T. G., Fraser-Smith, A. C., and Bernardy, A.: Results of ULF magnetic field measurements near the epicenters of the Spitak ($M_s=6.9$) and Loma Prieta ($M_s=7.1$) earthquakes: comparative analysis, *Geophys. Res. Lett.*, 19, 1495–1498, 1992.
- Molchanov, O. A. and Hayakawa, M.: Generation of ULF electromagnetic emissions by microfracturing, *Geophys. Res. Lett.*, 22, 3091–3094, 1995.
- Molchanov, O. A.: Fracturing as an underlying mechanism of Seismo-Electric Signals, in: *Atmospheric and Ionospheric Electromagnetic Phenomena Associated with Earthquakes*, edited by: Hayakawa, M., *Terra Sci. Publ. Comp.*, 349–356, 1999.
- Molchanov, O. A., Kulchitsky, A. V., and Hayakawa, M.: Inductive seismo-electromagnetic effect in relation to seismogenic ULF emission, *Nat. Haz. Earth Sys. Sc.*, 1, 61–67, 2001, **SRef-ID: 1684-9981/nhess/2001-1-61**.
- Molchanov, O. A., Schekotov, A., Fedorov, E., Belyaev, G., and Gordeev, E.: Preseismic ULF electromagnetic effect from observation at Kamchatka, *Nat. Haz. Earth Sys. Sc.*, 3, 1–7, 2003.
- Morgunov, V. A., Lubashevsky, M. N., Fubrizius, V. Z., and Fubrizius, Z. E.: Geoacoustic precursor of Spitak earthquake, *Volcanology and Seismology*, 4, 104–107, 1991.
- Saltykov, V. A., Sinitsyn, V. I., and Chebrov, V. N.: Variations of the tidal component in high-frequency seismic noise arising from changes in Earth stresses, *Volcanology and Seismology*, 19, 471–483, 1998.
- Scholz, C. H.: *The mechanics of earthquakes and faulting*, Cambridge University Press, 439, 1990.
- Surkov, V. V.: ULF electromagnetic perturbations resulting from the fracture and dilatancy in the earthquake preparation zone, *Atmospheric and Ionospheric Phenomena Associated with Earthquakes*, edited by: Hayakawa, M., TERRAPUB, 357–370, 1999.
- Takeuchi, N., Chubachi, N., and Narita, K.: Observation of earthquake waves by the vertical earth potential difference method, *Phys. Earth Planet. Inter.*, 101, 157–161, 1997.
- Uyeda, S., Nagao, T., Hattori, K. et al.: Japanese-Russian Complex Geophysical Observatory in Kamchatka region for monitoring of phenomena connected with seismic activity, in: *Seismo-Electromagnetics (Lithosphere-Atmosphere-Ionosphere Coupling)*, edited by: Hayakawa, M. and Molchanov, O., TerraPub, 413–420, 2002.